



HAL
open science

Satellite observations indicate slower recovery of woody components compared to upper-canopy and leaves in tropical rainforests after drought

Yujie Dou, Feng Tian, Jean-Pierre Wigneron, Xiaojun Li, Wenmin Zhang, Yaoliang Chen, Luwei Feng, Qi Xie, Rasmus Fensholt

► To cite this version:

Yujie Dou, Feng Tian, Jean-Pierre Wigneron, Xiaojun Li, Wenmin Zhang, et al.. Satellite observations indicate slower recovery of woody components compared to upper-canopy and leaves in tropical rainforests after drought. *Communications Earth & Environment*, 2024, 5 (1), pp.725. 10.1038/s43247-024-01892-9 . hal-04844676

HAL Id: hal-04844676

<https://hal.inrae.fr/hal-04844676v1>

Submitted on 18 Dec 2024

HAL is a multi-disciplinary open access archive for the deposit and dissemination of scientific research documents, whether they are published or not. The documents may come from teaching and research institutions in France or abroad, or from public or private research centers.

L'archive ouverte pluridisciplinaire **HAL**, est destinée au dépôt et à la diffusion de documents scientifiques de niveau recherche, publiés ou non, émanant des établissements d'enseignement et de recherche français ou étrangers, des laboratoires publics ou privés.



Distributed under a Creative Commons Attribution 4.0 International License

<https://doi.org/10.1038/s43247-024-01892-9>

Satellite observations indicate slower recovery of woody components compared to upper-canopy and leaves in tropical rainforests after drought

Check for updates

Yujie Dou^{1,2}, Feng Tian^{1,3,4}✉, Jean-Pierre Wigneron⁵, Xiaojun Li⁵, Wenmin Zhang⁶, Yaoliang Chen⁷, Luwei Feng¹, Qi Xie¹ & Rasmus Fensholt⁶

The 2015–2016 El Niño-induced drought caused biomass loss in global tropical forests, yet the recovery duration of different vegetation components (woody components, upper canopies, and leaves) remains unknown. Here, we use satellite remote sensing data of vegetation optical depth and leaf area index, with varying sensitivity to different vegetation components, to examine vegetation recovery during the drought event. We find that the woody component had the slowest recovery compared to the upper canopy and leaves, and displayed greater spatial variability between continents. Key factors influencing woody recovery include drought severity, moisture-related climatic conditions (i.e., vapor pressure deficit, precipitation, and soil moisture), and seasonal variations in temperature and precipitation. Our study highlights the importance of different vegetation components for maintaining ecosystem balance under drought disturbances and indicates the need for further research to explore recovery mechanisms and the long-term impacts of drought on forest dynamics.

Tropical ecosystems represent 34% of the global gross primary terrestrial productivity¹ and play a major role in carbon cycles at the global scale². However, the effectiveness of capturing and storing carbon to mitigate future global warming partly depends on the impact of severe drought episodes as water is the primary determinant of the amount and allocation of forest biomass production, and thereby the interannual variability of the tropical carbon cycle³. Droughts in tropical regions are predominantly associated with the El Niño-Southern Oscillation (El Niño), and many extreme drought events in tropical regions coincide with El Niño events¹. Notably the 2015–2016 El Niño led to historically high temperatures and low precipitation across the tropics, and the growth rate of atmospheric carbon dioxide was the largest on record⁵. An earlier study found that the carbon stocks in African and American humid forests had not recovered to pre- El Niño levels by 2017⁶, and the duration of the vegetation recovery period has yet to be determined.

Different vegetation components are characterized by differences in response time during drought conditions. Several experiments have demonstrated that the sensitivity of woody growth rate to drought surpasses that of vegetation canopy greenness⁷ because vegetation growth reduction is more mediated by the functional processes related to building a carbon sink than by the quantity of biomass synthesized through photosynthesis^{8,9}. However, these experiments were conducted at the species level, and the spatial variability in the sensitivity of different parts of woody plants remains unexplored.

Moreover, the response of forests to drought does not only depend on forest resistance and adaptation strategies, but is also highly dependent on the severity of drought events¹⁰, the time scale at which drought occurs¹¹, and the duration of the drought. For example, larger resistance to drought has been observed in spring when vegetation is in its reproductive stage, and productivity is at its peak¹¹. Tropical tall forests are found to be more

¹Hubei Key Laboratory of Quantitative Remote Sensing of Land and Atmosphere, School of Remote Sensing and Information Engineering, Wuhan University, Wuhan, China. ²Key Research Institute of Yellow River Civilization and Sustainable Development & Collaborative Innovation Center on Yellow River Civilization of Henan Province, Henan University, Kaifeng, China. ³Perception and Effectiveness Assessment for Carbon-neutrality Efforts, Engineering Research Center of Ministry of Education, Wuhan, China. ⁴Wuhan Institute of Quantum Technology, Wuhan, China. ⁵INRAE, UMR1391 ISPA, Université de Bordeaux, F-33140 Villenave d'Ornon, France. ⁶Department of Geosciences and Natural Resource Management, University of Copenhagen, Copenhagen, Denmark. ⁷Fujian Provincial Key Laboratory for Subtropical Resources and Environment, School of Geographical Sciences, Fujian Normal University, Fuzhou, China.

✉e-mail: tian.feng@whu.edu.cn

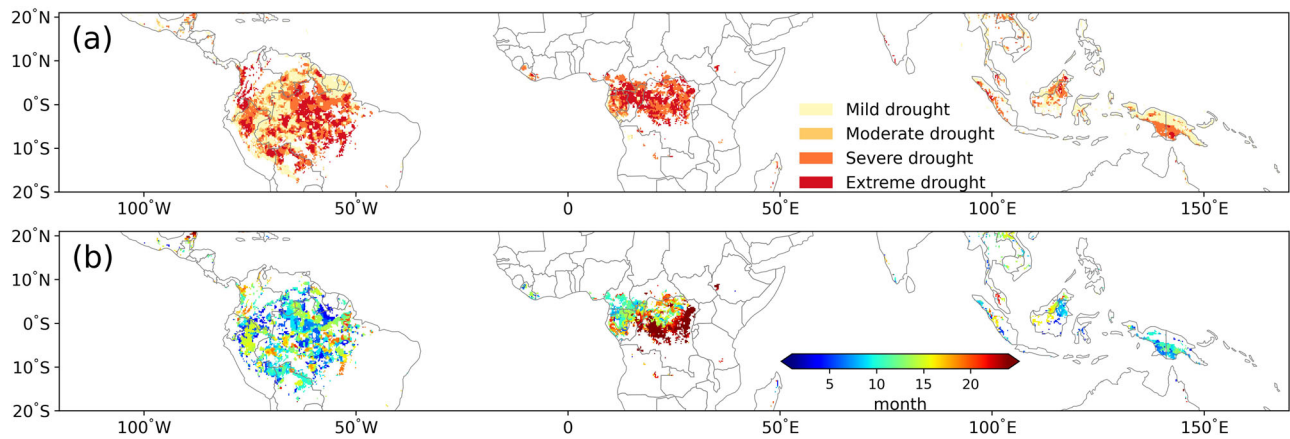


Fig. 1 | Spatial distribution of drought intensity and drought duration identified by SPEI. a Drought intensity and **b** drought duration. Mild drought ($-1 < \text{SPEI} \leq -0.5$), moderate drought ($-1.5 < \text{SPEI} \leq -1$), severe drought ($-2 < \text{SPEI} \leq -1.5$), and extreme drought ($\text{SPEI} \leq -2$).

sensitive and vulnerable to drought than short forests¹², and a higher species diversity could enhance drought resistance¹³. Therefore, to better understand drought impacts on tropical forest ecosystems, it is necessary to consider and incorporate information on forest traits, drought severity, and climate to investigate the potential drivers of forest recovery from drought.

Remote Sensing technology provides a powerful tool to investigate the vegetation dynamics from local to global scales. Optical-based multi-spectral remote sensing images have been used to derive a wide number of spectral vegetation indices based on reflectance ratios, which provide valuable insights into the photosynthetic vegetation component (e.g., herbaceous cover and leaves of woody plants). For example, the optical-based Leaf Area Index (LAI) quantifies the amount of leaf area within an ecosystem, serving as a critical variable in processes such as photosynthesis and respiration¹⁴. The Normalized Difference Water Index (NDWI) utilizes the Near-Infrared (NIR) and Short Wave Infrared (SWIR) channels to reflect changes in both water content (via SWIR radiation absorption) and the spongy mesophyll in vegetation canopies¹⁵. However, optical-based vegetation indices primarily identify changes in the leaves at the canopy, providing limited information about alterations in branches and the woody components of vegetation.

Microwave observations are less sensitive to atmospheric effects and are more sensitive to the water present in vegetation¹⁶, and the lower frequencies (i.e., longer wavelength) have improved capabilities of penetrating deeper into the vegetation layer. The vegetation optical depth (VOD) data was derived from multi-frequency passive microwave spaceborne observations, which is a parameter used for quantifying microwave transmissivity of the vegetation layer and is mainly determined by vegetation water content from both foliar and woody components^{17–19}. The L-band VOD (L-VOD, 1.4 GHz) has a lower frequency, allowing for deeper penetration into the vegetation layer²⁰ with minimal influence from green non-woody plant components^{19,21}. In contrast, the X-band VOD (X-VOD, 10.7 GHz) is sensitive to changes in the vegetation canopy, and it can serve as an independent bioclimatic growing season index compared to MODIS optical-based vegetation indices²². However, X-VOD cannot fully penetrate the entire canopy in forests with high tree height, such as in tropical evergreen broadleaf forests (EBF)²³. Therefore, it is considered as an indication of smaller branches and foliar of the upper canopy layer of EBF forest^{23,24}.

Here, we used satellite remote sensing data of L-VOD, X-VOD, and LAI as proxies for the woody component, particularly the branches, the upper canopies including canopy foliage and the branches at the top of the canopy, and the leaf component of tropical forest trees, respectively (Methods). To understand their respective sensitivity to drought, we aimed to investigate the recovery time of the different components of tropical EBF across the pan-tropics following the El Niño-induced drought of 2015–2016, by analyzing time series of satellite data from 2010–2022. We also employed the random forest method to ancillary data of climatic conditions, drought-

related information, and ecosystem-related factors to investigate the primary drivers of spatial variability in the recovery time of the vegetation component in tropical EBF.

Results

Severity of the 2015–2016 drought

The severity of drought was identified by standardized precipitation evapotranspiration index (SPEI) data. Most EBF in South America (56%) and Africa (90%) regions have experienced severe drought (i.e., $\text{SPEI} < -1.5$) (Fig. 1a) caused by the 2015–2016 El Niño, and there were obvious differences in the drought duration across the pan-tropical area (Fig. 1b). The EBF in Africa showed the most widespread exposure to long-duration droughts, with drought periods lasting up to 6 months covering 93% of the region, whereas 58% of South America forests and 40% of Asian forests have been exposed to such long-duration droughts, respectively.

Recovery time of different vegetation components

The reliability of using satellite remote sensing data to represent different vegetation components was validated through field experiments and empirical regression between canopy height and vegetation indices (VIs, including L-VOD, X-VOD, and LAI) (Methods and Supplementary Fig. S1). Specifically, L-VOD was shown to capture the woody components, particularly branches, while X-VOD reflected the upper canopy, including both foliage and branches at the top of the canopy. LAI, on the other hand, corresponded to the leaf component. Then, we calculated the recovery time of these three vegetation components by analyzing the time-series data of SPEI and VIs (Fig. 2 and Methods).

Noticeable spatial differences in the recovery time of the woody component, the upper canopy layer, and the leaves were observed following the 2015–2016 drought (Fig. 3). The recovery of the upper canopy layer and leaves was faster than the woody component. Nearly 73% of the upper canopy layer area and 92% of the leaf area recovered to the pre-El Niño conditions within two months, while only 52% of the drought-affected woody component area showed a similar recovery time (Table 1, Supplementary Fig. S2a). Moreover, there were 29% of the area for the woody component did not recover within one year (Supplementary Fig. S2a), whereas only 1% of the upper canopies were affected, with all the leaves being fully recovered within the same period. Notably, regardless of whether the calculations were performed on the resampled coarse spatial resolution or the original 500-meter spatial resolution, the LAI recovery time following drought events was consistently short, typically occurring within two months. Supplementary Fig S3 illustrates the recovery comparison of LAI in Africa, where greater temporal differences are observed compared to Asia and South America.

The recovery time of the upper canopy layer and the leaf component exhibited less spatial variation, but there were notable variations in the

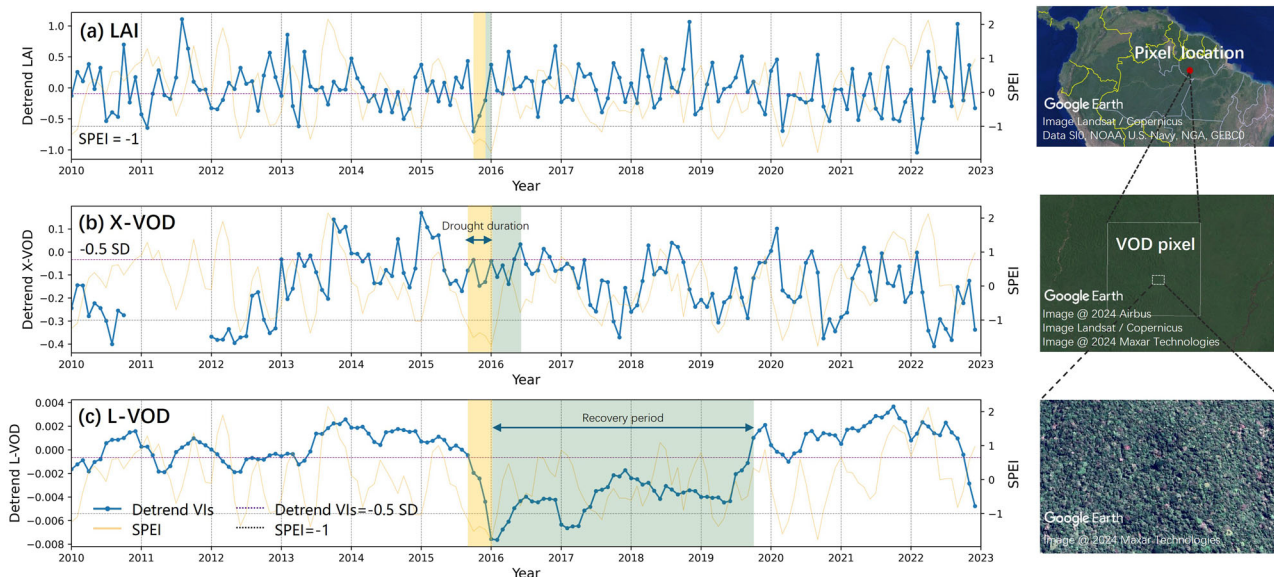


Fig. 2 | The identification of drought event and calculation of vegetation recovery for different components. Here is an example of the drought duration (yellow shaded) and recovery time (greening shaded) definition over an EBF pixel in South America (0.5° S, 57° W). Leaves were quantified by (a) LAI, the upper canopies were quantified by (b) X-VOD, and the woody component was quantified by (c) L-VOD. The maps on the right column are from Google Earth.

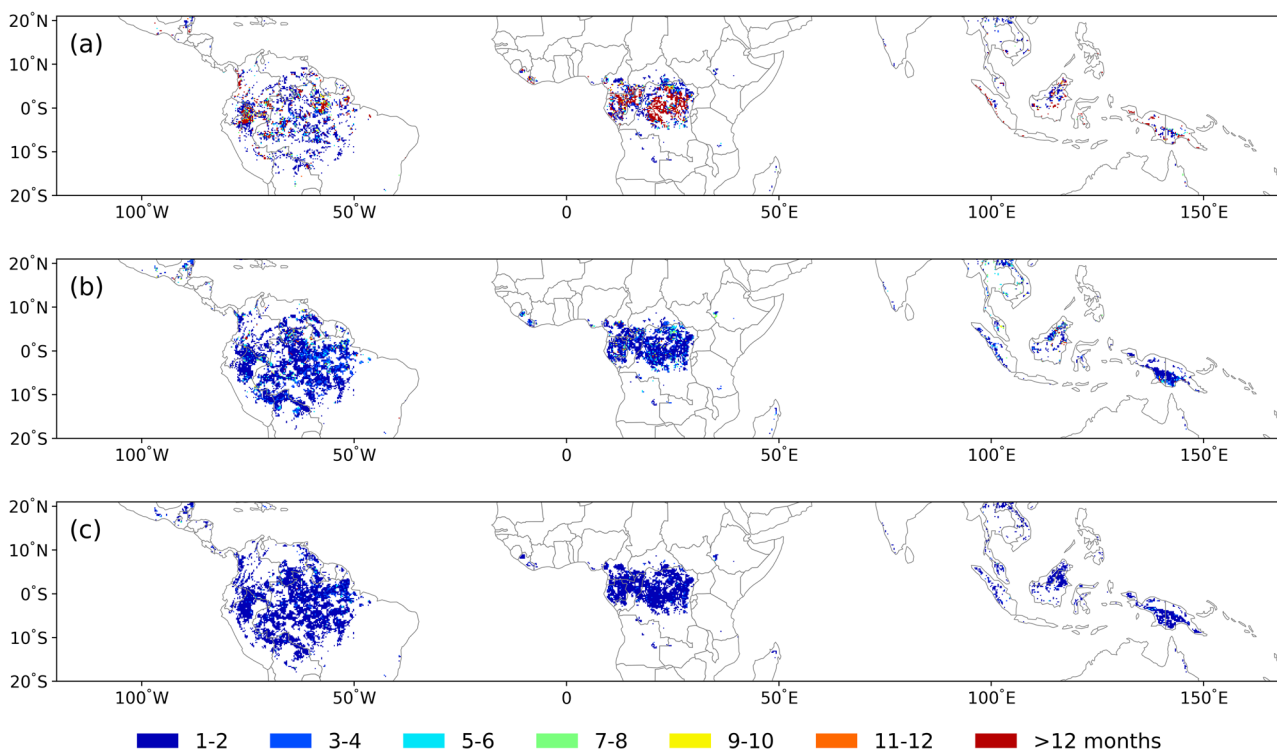


Fig. 3 | Spatial distribution of the recovery time for different vegetation components after drought. a The woody component, b the upper canopy layer, and c leaves.

recovery time of the woody components in the forest regions of South America, Africa, and Asia. The woody components of EBF in South America show the fastest recovery (Fig. 3a), with 57% of the region recovering within 2 months. The recovery time for EBF in Africa is the longest, with 42% of the region requiring more than 12 months to fully recover.

As for the recovery time for different vegetation components, the pixel scale leaf component recovers first, followed by the upper canopy layer and the woody components (Fig. 3, Supplementary Fig. S2, S4). In 93.8% of forested areas, the leaf component showed simultaneous recovery time with either the upper canopy layer, the woody component, or both (in 12.6% of

the study area, the leaf component recovered first preceding the recovery of the upper canopy layer and the woody component) (Fig. 3b). This phenomenon was common in South America, Africa, and Asia (Supplementary Fig. S4). The regions where the upper canopy layer showed simultaneous recovery time with either the leaf component, the woody component, or both account for 72.7% (in 2.3% of forested areas, the upper canopy layer recovered first preceding the recovery of the other two components). Nearly 37.8% of forested areas showed simultaneous recovery time of the woody component with either the leaf component, the upper canopy layer, or both (the areas where the woody component recovered first account for 2%). It is

Table. 1 | Area percentage of the recovery time for different vegetation components across tropical EBF regions

Components	<= 2	3 – 4	5 – 6	7 – 8	9 – 10	11 – 12	>12 months
Leaves	92%	6.5%	1.1%	0.3%	0.1%	0	0
Upper Canopy	72.9%	17%	5.6%	2.3%	0.8%	0.4%	1%
Woody Component	51.9%	7.2%	5.2%	3.2%	2.3%	1.5%	28.6%

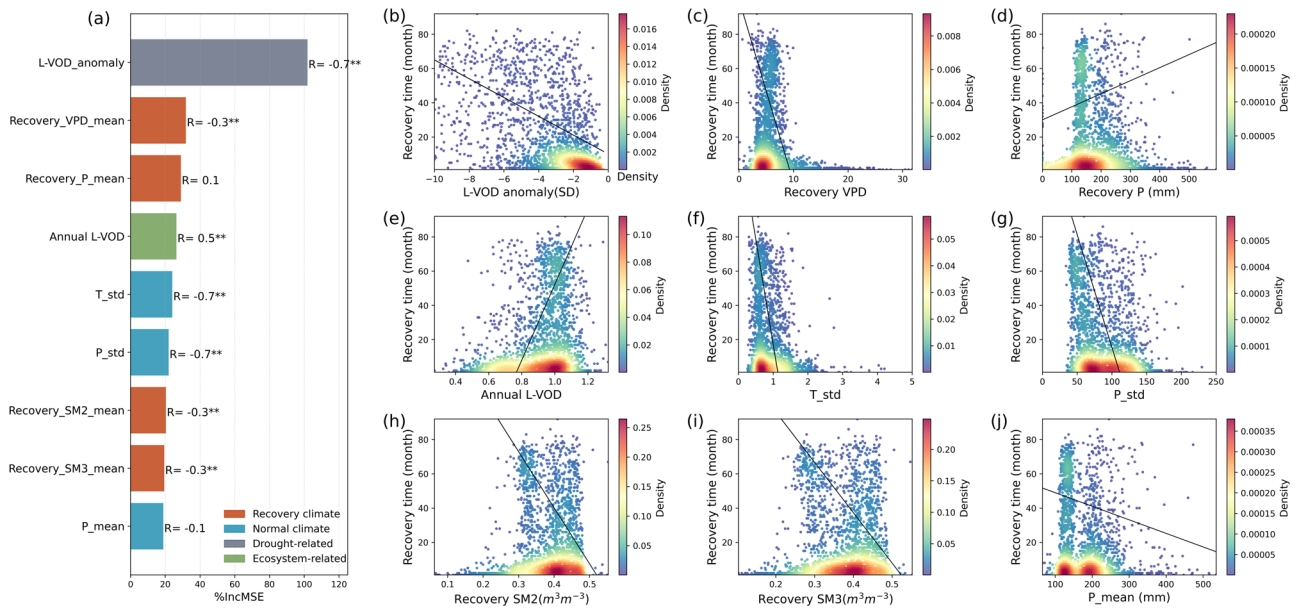


Fig. 4 | Attributions of the normal climatic conditions, climatic conditions during the woody recovery period, drought-related, and ecosystem-related factors to the recovery time of the woody component across tropical evergreen broadleaf forests. **a** The relative importance of the predictor variables in the random forest model is shown by the percentage increase of mean squared error (%IncMSE). The scatterplots illustrate the relationships between the woody recovery time and various factors, **b** L-VOD anomaly during the drought period, **c**, **d** mean monthly

VPD and precipitation during the recovery period, **e** annual L-VOD pre-El Niño period, **f**, **g** monthly temperature and precipitation variation, **h**, **i** mean monthly soil moisture layer 2 and layer 3 during the recovery period, and **j** the long-term mean monthly precipitation. *R* indicates the correlation coefficient between the recovery period and the influencing factors. Asterisks denote significant linear correlations at 0.01 “**” and 0.05 “*” levels, respectively.

important to note that we do not assume that these components recover independently of each other. After a drought event, different vegetation components such as leaves, the upper canopies, and the woody component recover simultaneously, but the recovery time for each is distinct.

Main drivers of woody component recovery across global tropical rainforests

The random forest regression model was used to investigate the drivers of woody component recovery across tropical rainforests (Methods). The input factors (including drought severity, moisture-related climatic conditions, and seasonal variations) incorporated in the random forest model collectively explained 70% of the variability in the woody component recovery across the tropical region of EBF forests. The severity of the drought impact on the woody component (i.e. L-VOD anomaly) emerged as the primary determinant of the recovery time (%IncMSE = 102%) (Fig. 4a). Moreover, there was a significant negative correlation between L-VOD anomalies and the recovery time of the woody component ($R = -0.58, p < 0.01$), indicating that more severe impacts of drought on the woody component result in longer recovery time (Fig. 4b). Subsequently, the climatic conditions related to moisture levels during the recovery period, including mean monthly vapor pressure deficit (VPD) (%IncMSE = 32%, $R = -0.13, p < 0.01$) and mean monthly precipitation (%IncMSE = 29%, $R = 0.03, p < 0.05$), were found to be important explanatory variables of the recovery time. Biomass (i.e. annual L-VOD) is also closely related to the recovery of vegetation woody components (%IncMSE = 26%, $R = 0.27,$

$p < 0.01$). The higher the vegetation biomass, the longer the corresponding recovery time.

The seasonal variation (i.e., the standard deviation of monthly air temperature and precipitation) also played an important role in influencing the recovery of the vegetation woody component. When the seasonal showed minor variations (e.g., smaller standard deviations in monthly temperature (%IncMSE = 32%, $R = -0.24, p < 0.01$) and monthly precipitation (%IncMSE = 32%, $R = -0.29, p < 0.01$)), the recovery time of the woody layer tended to be prolonged. Finally, soil moisture (SM) of layer 2 during the recovery period (%IncMSE = 20%, $R = 0.02, p > 0.05$), soil moisture of layer 3 during the recovery period (%IncMSE = 19%, $R = -0.03, p > 0.05$), and the long-term mean monthly precipitation (%IncMSE = 19%, $R = -0.12, p < 0.01$) also positively contributed to the recovery of the woody component, with more water availability corresponded to shorter recovery time.

We also analyzed the primary influencing factors on the woody component recovery time of EBF in South America (56% explanation), Africa (73% explanation), and Asia (54% explanation) separately (Supplementary Fig. S5–S7). We found that the severity of the drought impact on the woody component (i.e. L-VOD anomaly) consistently remained the most significant factor affecting the recovery time of the woody component over all three continents. This was followed by the climatic conditions during the recovery period in South America and Africa, as well as the drought-related factors (e.g. air temperature anomaly, VPD anomaly) in Asia.

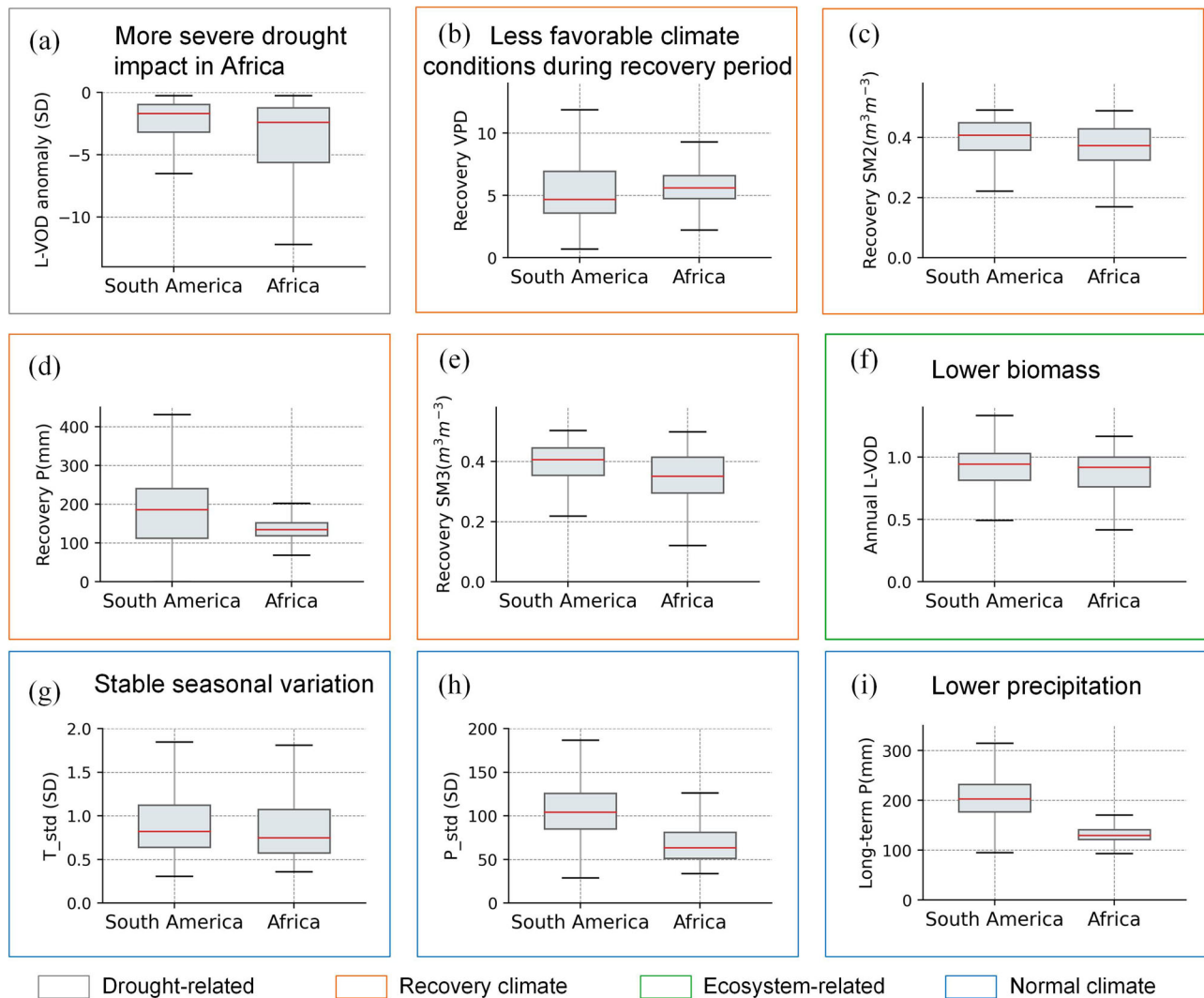


Fig. 5 | Statistical distribution of the main influencing factors on the recovery of the woody component in South America and Africa. **a** L-VOD anomaly during the drought period, **b–e** mean monthly VPD, precipitation, soil moisture of layer 2 and layer 3 during the recovery period, **f** annual L-VOD before El Niño, **g, h** seasonal

variation in monthly temperature and precipitation variation, and **i** the long-term monthly mean precipitation. The horizontal lines at the top and bottom of the box plot represent the 25th and 75th percentiles, respectively, while the red line indicates the median.

We also analyzed the primary factors influencing the recovery time of the upper canopy and leaves in tropical EBF forests. Our findings showed that the input factors incorporated in the random forest model explained only 9% and 7% of the variability in the recovery time of the upper canopy and leaves, respectively, across the tropical EBF forests (Supplementary Fig. S8–S9). This limited explanatory power may be due to the non-continuous variables of recovery time, as well as the relatively low range of recovery time values observed for the upper canopy and the leaves. Therefore, we did not provide a detailed analysis of the primary factors influencing the upper canopy and leaves in this study.

Explanations for the faster recovery of the woody component in South America compared to Africa

The primary drivers of the woody components recovery in rainforests worldwide could well explain why these components recovered more quickly in South America than in Africa. Firstly, the severity of the drought impact on the woody component (i.e. L-VOD anomaly) was more pronounced in Africa than in South America (mean L-VOD anomaly = -3.0 SD in Africa vs. -2.3 SD in South America) (Fig. 5a). In Africa, the most negative impact of drought on the woody component was concentrated in

the Congo Rainforest region, where the L-VOD anomaly was lower than in other regions (Supplementary Fig. S10).

Secondly, the climatic conditions related to moisture levels during the recovery period in South American EBF regions were more favorable than in Africa with lower VPD (mean VPD = 5.9 in South America vs. 6.3 in Africa), more precipitation (mean precipitation = 182 mm in South America vs. 136 mm in Africa), and more soil moisture (mean soil moisture of layer 2 = $0.39 \text{ m}^3 \text{ m}^{-3}$ in South America vs. $0.37 \text{ m}^3 \text{ m}^{-3}$ in Africa, mean soil moisture of layer 3 = $0.39 \text{ m}^3 \text{ m}^{-3}$ in South America vs. $0.35 \text{ m}^3 \text{ m}^{-3}$ in Africa) (Fig. 5b–e). The pre-El Niño annual VOD in EBF of South America was slightly higher than in Africa (mean pre-El Niño annual VOD = 0.91 in South America vs. 0.87 in Africa) (Fig. 5f), but the impact of drought on the woody component and the influence of climate on the recovery period is greater than that of biomass alone (Fig. 4a). Therefore, solely comparing biomass values cannot adequately explain why the recovery time of the woody vegetation layer in South America is faster than that in Africa.

Finally, the EBF in Africa showed a more stable seasonal variation with lower monthly temperature variation (mean temperature variation = 0.9 SD in South America vs. 0.88 SD in Africa) and monthly precipitation variation (mean precipitation variation = 106 SD in South America vs. 71 SD in Africa). Additionally, the EBF has lower precipitation availability in Africa

than South America (mean precipitation = 207 mm in South America vs. 137 mm in Africa). Therefore, the severity of drought impact on the woody component, the less favorable moisture-related climatic conditions during recovery, and the smaller seasonal variation in Africa compared to South America's EBF contribute to a slower recovery of the woody component in Africa compared to South America.

It should be noted that due to the relatively smaller area of EBF in Asia compared to South America and Africa, we chose only to focus our analysis on understanding the differences in the recovery time of woody components in vegetation between South America and Africa.

Discussion

We used L-VOD, X-VOD, and LAI data separately as proxies of the woody component (i.e. branches), the upper canopy layer (including canopy foliage and branches at the top of the canopy), and the leaf component to investigate the recovery of these components in tropical EBF regions during the extreme drought period induced by the 2015–2016 El Niño event. We found that the recovery time of the leaf component is the fastest, followed by the upper canopy layer and the woody component (Fig. 3, Supplementary Fig. S2, S4).

During a drought period, the leaf component initially responds by closing stomata. This is followed by a response in the woody component²⁵, such as reduced xylem water transport efficiency, possible embolism formation, and altered turgor pressure. These effects can decrease hydraulic conductivity, impair water transport from roots to leaves, and stress the plant's structural integrity, potentially damaging woody tissues. Although the longstanding theory holds that stomata optimize fitness by maintaining constant marginal water use efficiency over a specified time frame, a recent evolutionary theory suggests an alternative perspective that stomata aim to maximize the carbon gain while minimizing carbon costs and the risk of hydraulic damage¹³. Additionally, vegetation typically adjusts biomass allocation by directing more resources to the underground parts to capture additional water in deep soil layers during drought periods, thereby reducing water stress, with the woody component receiving a minimum biomass allocation²⁶. Moreover, non-photosynthetic (woody) and photosynthetic (foliar) canopy biomass exhibit slower recovery rates²⁷. The leaves of vegetation, which represent the primary source of photosynthesis in plants, are highly responsive to changes in the photosynthetic process. Given the current atmospheric CO₂ levels, drought primarily limits tree growth by affecting radial growth and structural development, rather than by limiting biomass production through photosynthesis⁸. Furthermore, the woody component has been revealed to be the most sensitive component to drought compared to litterfall and below-ground parts²⁸. This high sensitivity of the woody component leads to a greater reduction in overall vegetation growth during drought, compared to the impact on leaves⁷. Therefore, the recovery of the woody component is slower compared to that of the leaf component (Fig. 3).

The moisture-related climatic conditions during the recovery period have a substantial impact on the recovery of the vegetation woody component. The mean monthly VPD, precipitation, and the soil moisture of layer 2 and layer 3 were identified as the most influencing climatic factors affecting the recovery of the vegetation woody component (Fig. 4). The strong impact of moisture-related climatic conditions during the recovery period on the recovery of woody component partly depends on the sensitivity of vegetation to specific climatic factors. For example, VPD modulates hydraulic function and structure in tropical rainforests during the recovery period with sufficient soil water supply²⁹, making tall Amazon forests more sensitive to VPD than precipitation³⁰. Soil moisture supplies the water resource to tropical forests and thus is a key controller of tropical forest local hydrology³¹.

The adaptability of vegetation to normal climate conditions also influences the recovery of vegetation woody components. Vegetation tends to become more adaptive to climate change in regions with higher seasonal variations³². Thus, the EBF of South America experiences greater seasonal variations with higher monthly precipitation and temperature variation

(Fig. 5g, h), allowing vegetation to adapt well to climate changes and correspondingly resulting in shorter recovery times (Figs. 3, 4). Moreover, the EBF in Africa is more accustomed to drought and therefore exhibits greater resilience to droughts³³, which also implies that when Africa experiences severe drought events, it will require more time for recovery (Fig. 3).

There is a significant positive correlation between biomass and the recovery of the woody component in tropical EBF (Fig. 4a). As biomass increases, the duration required for recovery also increases. This tendency may be attributed to higher biomass levels in the study area aligning with enhanced ecosystem diversity, facilitated by the diversity of plant hydraulic strategies and traits that can buffer a forest ecosystem against drought. Therefore, heightened biodiversity correlates with increased resilience to drought¹³, resulting in prolonged recovery periods. However, in this study, since biomass is not the most important influencing factor on the recovery of the woody component, it is therefore not appropriate to solely compare the recovery times of the woody vegetation component in different regions based on biomass alone.

VOD data from different frequencies enables monitoring of vegetation recovery in tropical forests, but some limitations still exist. Although L-VOD can penetrate the whole vegetation layer, it may not fully represent changes in vegetation biomass in tropical regions with dense forests³⁴. Although phenological information extracted from X-VOD shows good consistency with that obtained from optical methods in tropical rainforest regions with dense biomass³⁵, X-VOD still exhibits saturation problems in these areas^{36,37}.

Furthermore, since this study focuses on recovery time calculations at a monthly scale, we cannot well compare the recovery time of the upper canopy and leaves in nearly half of the EBF regions as they were fully recovered within one month. Additionally, it is important to note that our study focuses on EBF regions, but even though EBF is the dominant land cover within the VOD pixels, it might not be the only type. The land cover within each VOD pixel (0.25°) is not entirely homogeneous, and different plant types may exhibit varying recovery mechanisms. For example, after drought, anisohydric species may maintain positive carbon gains for a longer period as rainfall returns, allowing them to survive longer until they reach the threshold of carbon starvation³⁸. Therefore, the coarse spatial resolution of VOD introduces uncertainties in calculating recovery duration. Moreover, the accuracy errors in VOD data for tropical rainforests can also introduce uncertainty in the calculation results of recovery time. For example, the smaller scattering effect during a drought period or dry season compared to normal conditions may result in elevated L-VOD estimations³⁹, thereby delaying the immediate observation of the drought's impact on vegetation. Therefore, we acknowledge that there may be some uncertainty in the calculations of the recovery time for the three vegetation components after drought, as we performed these calculations at a monthly time scale and with a spatial resolution of 0.25°. Given that long-term and high spatial-resolution VOD data products are currently unavailable, we welcome future higher spatial-resolution VOD datasets to refine the study of vegetation recovery from drought.

Despite these challenges, VOD data from different frequencies possess unique advantages in observing vegetation structures, and further improving the accuracy of VOD estimations and the spatial resolution is expected to bring additional benefits in research focusing on tropical rainforest areas, including but not limited to vegetation biomass carbon estimation and vegetation water content variation monitoring.

Conclusion

In this study, we employed L-VOD, X-VOD, and LAI as proxies for the woody component, the upper canopy layer, and the leaf component of vegetation, respectively, to examine the recovery time of these vegetation elements in tropical forest regions following the 2015–2016 El Niño-induced drought. We found that the leaf component demonstrated a quicker recovery from drought, followed by the upper canopy layer and the woody component. Notably, the recovery time of the vegetation woody component exhibited greater spatial heterogeneity than the other two vegetation components. The recovery time of the woody component was primarily

influenced by the impact of drought on the woody component, followed by the moisture-related climatic conditions during the recovery period (i.e., VPD, precipitation, and soil moisture) and the magnitude of the seasonal variation (i.e. the magnitude of the standard deviations in monthly temperature and precipitation). The more severe the damage to the woody component of vegetation during a drought, the less favorable the climate conditions during the recovery period (i.e., less precipitation, lower soil moisture, and higher VPD), and the higher the seasonal variations (i.e. larger standard deviations in monthly temperature and precipitation), the longer the corresponding recovery time for the woody component of vegetation. Therefore, due to the more extensive impact on the woody component during drought in Africa compared to South America, coupled with less favorable moisture-related climatic conditions during the post-El Niño recovery period and lower seasonal variation (i.e. larger standard deviations in monthly temperature and precipitation) in Africa than in South America, the recovery time of the woody component in Africa exceeded that in South America.

Methods

Tropical evergreen broadleaf forest region

The study region is situated within the tropical evergreen broadleaf forest (EBF) zone, encompassing tropical EBF areas in South America, Africa, and Asia (Supplementary Fig. S11). To identify the tropical EBF region, the MODIS International Geosphere-Biosphere Program (IGBP) classification scheme Version 6.1 data were used to delineate the tropical EBF region. We excluded the VOD pixels dominated by non-EBF using the aggregated 25 km MODIS land cover map from 2010 to 2022. Areas within VOD footprints where urban and cropland cover exceeds 5% were masked. Furthermore, considering the potential impact of urban and cropland expansion on vegetation monitoring, we also excluded pixels with proportions of urban and cropland expansion exceeding 5% from 2010 to 2022 using MODIS land cover data, as well as pixels with forest loss exceeding 5% from 2015 to 2022 based on Hansen's global forest change data⁴⁰ to exclude large deforestation event. Considering that the occurrence of fires in tropical rainforests is relatively low, this study did not take fire variability into account when defining the study area.

Vegetation indices data

The SMOS-SMAP-INRAE-BORDEAUX (SMOSMAP-IB) L-VOD product was retrieved from temperature brightness observed from ESA's Soil Moisture Ocean Salinity (SMOS) and NASA's Soil Moisture Active Passive (SMAP). It offers L-VOD at a semi-daily temporal resolution and a grid resolution of 25 km⁴¹. The semi-daily global LPDR X-VOD dataset at 0.25° spatial resolution, derived from AMSR-E (Advanced Microwave Scanning Radiometer – Earth Observing System) and AMSR-2 (Advanced Microwave Scanning Radiometer – 2) sensors³⁶ was also employed. Both nighttime L-VOD (ascending orbit, 6:00 AM) and X-VOD (descending orbit, 1:30 AM) were aggregated to monthly data by averaging, covering the period from 2010 to 2022. The MODIS LAI data Version 6.1 with 500 m spatial resolution from 2010 to 2022 was used, with monthly LAI data aggregated by taking the maximum values. All the vegetation index data have been converted to a geographic coordinate system format (i.e., WGS1984) with a spatial resolution of 0.25°. L-VOD and MODIS LAI data were resampled to 0.25° by averaging. Details regarding the validation of the vegetation indices data are provided in Supplementary Note S1.

Drought data

We used the Standardized Precipitation Evapotranspiration Index (SPEI) as a drought indicator to assess the emergence, length, and intensity of drought events. As the humid forest has been shown to respond to drought within three months⁴², the SPEI03 data with 0.05° spatial resolution⁴³ was selected, which was calculated from Multi-Source Weighted-Ensemble Precipitation (MSWEP) and potential evapotranspiration (PET) from the Global Land Evaporation Amsterdam Model (GLEAM). The SPEI03 is calculated by factoring in the past 3-month aggregated precipitation and potential

evapotranspiration, thus reflecting relatively short-term moisture conditions⁴⁴. The SPEI data were resampled to the spatial resolution of VOD data at 0.25° by averaging.

Ancillary data

Monthly air temperature, dewpoint temperature, and soil moisture data at 0.1° resolution from 2010 to 2022 were taken from the ERA5 monthly average reanalysis dataset. The soil moisture data covers three layers, including layer 1 (0–7 cm), layer 2 (7–28 cm), and layer 3 (28–100 cm). The air temperature and dewpoint temperature were used to calculate the vapor pressure deficit (VPD) using the method provided by Yuan et al.⁴⁵. The precipitation data was derived from the MSWEP product with a 3 h temporal resolution and 0.1° spatial resolution from 1979 to the present⁴⁶. All the climate data mentioned above were resampled to the spatial resolution of VOD data by averaging.

We included the “elasticity of substitution” data, which reflects the degree to which various species can substitute each other in enhancing forest productivity⁴⁷, the magnitude of the intrinsic variability of vegetation water content data to represent vegetation water buffering³⁴, and a proxy for vegetation biomass data (i.e. the mean annual L-VOD pre- El Niño year). Note that the mean annual VOD before El Niño was computed as the 95th percentile of nighttime VOD from 2010 to 2014 as recommended³⁴.

A high-resolution canopy height data at 10 m spatial resolution⁴⁸ was used to verify the representation of different vegetation indices for different vegetation components.

Representative of vegetation indices for different vegetation components

A field experiment performed in a deciduous forest showed minimal variation in L-band transmissivity between foliated and defoliated states, with the canopy being semi-transparent at these frequencies, making branches the dominant emitters at L-band frequency^{49,50}. In contrast, at X-band frequency, the canopy was opaque when foliated and became semi-transparent during defoliation, so they concluded that leaves are the main source of radiation at this wavelength⁴⁹. While X-band penetration changes appear to be driven by leaf cover, they could also result from phenological shifts as the water content in branches fluctuates with phenology³⁹, particularly in branches at the top of the canopy. Thus, X-band variations may not be solely attributable to leaf cover changes.

The relationships between canopy height and L-VOD, X-VOD, and LAI were built to verify further the sources that affected the X-band transmissivity (Supplementary Fig. S1). We found that whether using Locally Weighted Polynomial (LOESS)⁵¹ or Generalized Additive Model (GAM)⁵² nonlinear fitting, when the slope of the function approaches zero (i.e., at the saturation point), meaning that as VODs or LAI continues to increase, the change in canopy height becomes negligible. At this point, the canopy height corresponding to LAI is the lowest (27.8 m for LOESS fitting, and 26.6 m for GAM fitting), while the canopy height corresponding to L-VOD is the highest (35.3 m for LOESS fitting, and 34.2 m for GAM fitting). This suggests that X-VOD (30.7 m for LOESS fitting, and 28.5 m for GAM fitting) also contains signals related to major vegetation branches, especially at the top of the canopy.

Therefore, satellite remote sensing data for L-VOD, X-VOD, and LAI were utilized as proxies for different components of tropical forest trees: L-VOD represented the woody components, particularly the branches; X-VOD reflected the upper canopy, including both foliage and branches at the top of the canopy; and LAI corresponded to the leaf component.

Calculation of the recovery time

Monthly SPEI and vegetation indices (VIs, i.e. L-VOD, X-VOD, and LAI) were used together to identify drought events and the calculation of recovery time for different vegetation components at pixel-scale^{53,54}. The monthly VIs time-series data were deseasonalized by subtracting the monthly average values (calculated from the full period excluding the drought years from 2015 to 2016) from the VIs time series to remove the effects of the seasonal cycle and then detrended to eliminate the long-term trend. When a drought

event happens and the standardized deviation (SD) of the detrended VI data falls below -0.5 SD, the vegetation is considered to have been negatively affected by the drought event⁵⁴.

The drought event was considered to begin when the SPEI was lower than -1 and the detrended VI data at the same time were below -0.5 SD, and it ended when the SPEI was higher than -1 and the detrended VIs data remained below -0.5 SD, or SPEI stayed lower than -1 but the detrended VIs data increased above -0.5 SD. Additionally, we only focused on drought events lasting for at least 2 months (Fig. 2a–c).

The calculation of the drought recovery time for different vegetation components is based on the following criteria⁵⁴: (1) If the detrended VI data reached a local minimum during the drought period (see above), the recovery time was defined as the period from the time when the detrended VI data reached the minimum value to the time when the detrended VI data were higher than -0.5 SD (Fig. 2c). (2) If the condition above was not met, the recovery time was defined as the period from the end of the drought event (see above) to the time when the detrended VI data were larger than -0.5 SD (Fig. 2a, b).

Drivers of the recovery of vegetation woody component

We collected 44 response variables in the random forest regression model to investigate the relative significance of these variables to the recovery time of the three vegetation components. The 44 response variables were reclassified into four classes, including the normal climatic conditions, the climatic conditions during the recovery period, drought-related factors, and ecosystem-related factors.

Specifically, the variables covering the normal climatic conditions comprise annual mean, 25th percentile minimum, 75th percentile maximum, and standard deviation of air temperatures (T_{mean} , $T_{\text{min}25}$, $T_{\text{max}75}$, T_{std}), precipitation (P_{mean} , $P_{\text{min}25}$, $P_{\text{max}75}$, P_{std}), soil moisture from layers 1 to 3 ($SM1_{\text{mean}}$, $SM1_{\text{min}25}$, $SM1_{\text{max}75}$, $SM1_{\text{std}}$, $SM2_{\text{mean}}$, $SM2_{\text{min}25}$, $SM2_{\text{max}75}$, $SM2_{\text{std}}$, $SM3_{\text{mean}}$, $SM3_{\text{min}25}$, $SM3_{\text{max}75}$, $SM3_{\text{std}}$), and VPD (VPD_{mean} , $VPD_{\text{min}25}$, $VPD_{\text{max}75}$, VPD_{std}), covering the period from 2010 to 2022, excluding 2015 to 2016. The standard deviation of air temperatures, precipitation, soil moisture, and VPD were defined as the seasonal variation of normal climate conditions in this study.

The variables denoting the climatic conditions during the recovery period include monthly mean air temperature ($\text{Recovery}_T_{\text{mean}}$), precipitation ($\text{Recovery}_P_{\text{mean}}$), VPD ($\text{Recovery}_VPD_{\text{mean}}$), and soil moisture from layers 1 to 3 ($\text{Recovery}_SM1_{\text{mean}}$, $\text{Recovery}_SM2_{\text{mean}}$, $\text{Recovery}_SM3_{\text{mean}}$).

Drought-related factors encompass drought duration, drought severity (i.e. mean SPEI), the number of dry months (monthly precipitation less than 100 mm), anomalies of the climatic conditions relative to the pre-El Niño period, including temperature (T_{anomaly}), precipitation (P_{anomaly}), VPD (VPD_{anomaly}), and soil moisture from layer1 to layer3 ($SM1_{\text{anomaly}}$, $SM2_{\text{anomaly}}$, $SM3_{\text{anomaly}}$), and the severity of the drought impact on the woody component (i.e. the L-VOD anomaly during the drought period relative to the pre-drought condition, $L\text{-VOD}_{\text{anomaly}}$).

Ecosystem-related variables include the magnitude of the intrinsic variability of vegetation water content data representing vegetation water buffering ($\text{Mean}_{\text{delta}}_{\text{VOD}_{\text{day}}}$), biomass (i.e. pre-El Niño annual VOD values, annual L-VOD), and the elasticity of substitution.

The random forest regression model can explain interactions and nonlinear relationships between predictors⁵⁵. The importance of each response variable was assessed through the percentage increase in the mean square error (%IncMSE) between target and response values⁵⁶. The values of the %IncMSE were generated from a random forest model consisting of 500 decision trees in this study, and higher values of %IncMSE suggest higher importance of the response variables. It should be noted that random forest is a tree-based ensemble model that is sensitive to the nonlinear relationships and interactions among features. Therefore, even if a feature shows high importance in terms of

%IncMSE”, its coefficient of determination between recovery time and the response variables may not necessarily be high⁵⁷. Additionally, we conducted a principal component analysis (PCA) on the input data to transform highly correlated input factors (e.g., precipitation and VPD) into a set of uncorrelated principal components to mitigate the impact of collinearity. These principal components were used as the new input features for training the random forest model.

Data availability

The SMOSMAP-IB L-VOD data is available on the SMOS website <https://ib.remote-sensing.inrae.fr/>. LPDR X-VOD data can be freely accessed from the website <http://files.ntsg.umd.edu/data/>. MODIS data for LAI and land cover, as well as Hansen forest change data and canopy height, are accessible via the Google Earth Engine platform. The MSWEP precipitation product can be obtained from <http://www.gloh2o.org>. The SPEI data is available at <https://doi.org/10.5285/ac43da11867243a1bb414e1637802dec>. The ERA5 datasets for air temperature, dewpoint temperature, and soil moisture can be downloaded from <https://cds.climate.copernicus.eu/datasets>. The elasticity of substitution data is accessible at <https://www.gfbinitiative.org/data>.

Code availability

All codes utilized in this study are accessible upon request.

Received: 22 May 2024; Accepted: 8 November 2024;

Published online: 20 November 2024

References

- Beer, C. et al. Terrestrial gross carbon dioxide uptake: global distribution and covariation with climate. *Science* **329**, 834–838 (2010).
- Bonal, D., Burban, B., Stahl, C., Wagner, F. & Hérault, B. The response of tropical rainforests to drought—lessons from recent research and future prospects. *Ann. For. Sci.* **73**, 27–44 (2016).
- He, B., Xie, X. & Guo, L. A shift from temperature to water as the primary driver for interannual variability of the tropical carbon cycle. *Geophys. Res. Lett.* **50**, e2023GL102812 (2023).
- Marengo, J. A., Tomasella, J., Alves, L. M., Soares, W. R. & Rodriguez, D. A. The drought of 2010 in the context of historical droughts in the Amazon region: DROUGHT AMAZON 2010. *Geophys. Res. Lett.* **38**, n/a–2 (2011).
- Liu, J. et al. Contrasting carbon cycle responses of the tropical continents to the 2015–2016 El Niño. *Science* **358**, eaam5690 (2017).
- Wigneron, J.-P. et al. Tropical forests did not recover from the strong 2015–2016 El Niño event. *Sci. Adv.* **6**, eaay4603 (2020).
- Gazol, A. et al. Forest resilience to drought varies across biomes. *Glob. Change Biol.* **24**, 2143–2158 (2018).
- Sarris, D., Christodoulakis, D. & Körner, C. Recent decline in precipitation and tree growth in the eastern Mediterranean. *Glob. Change Biol.* **13**, 1187–1200 (2007).
- Zhang, Z. et al. Converging climate sensitivities of European forests between observed radial tree growth and vegetation models. *Ecosystems* **21**, 410–425 (2018).
- Taeger, S., Zang, C., Liesebach, M., Schneck, V. & Menzel, A. Impact of climate and drought events on the growth of Scots pine (*Pinus sylvestris* L.) provenances. *For. Ecol. Manag.* **307**, 30–42 (2013).
- Hahn, C., Lüscher, A., Ernst-Hasler, S., Suter, M. & Kahmen, A. Timing of drought in the growing season and strong legacy effects determine the annual productivity of temperate grasses in a changing climate. *Biogeosciences* **18**, 585–604 (2021).
- Liu, L. et al. Tropical tall forests are more sensitive and vulnerable to drought than short forests. *Glob. Change Biol.* **28**, 1583–1595 (2022).
- Anderegg, W. R. L. et al. Hydraulic diversity of forests regulates ecosystem resilience during drought. *Nature* **561**, 538–541 (2018).
- Fang, H., Baret, F., Plummer, S. & Schaepman-Strub, G. An overview of Global Leaf Area Index (LAI): methods, products, validation, and applications. *Rev. Geophys.* **57**, 739–799 (2019).

15. Gao, B. NDWI—A normalized difference water index for remote sensing of vegetation liquid water from space. *Remote Sens. Environ.* **58**, 257–266 (1996).
16. Konings, A. G., Rao, K. & Steele-Dunne, S. C. Macro to micro: microwave remote sensing of plant water content for physiology and ecology. *N. Phytol.* **223**, 1166–1172 (2019).
17. Cui, Q., Shi, J., Du, J., Zhao, T. & Xiong, C. An approach for monitoring global vegetation based on multiangular observations from SMOS. *IEEE J. Sel. Top. Appl. Earth Observations Remote Sens.* **8**, 604–616 (2015).
18. Shi, J. et al. Microwave vegetation indices for short vegetation covers from satellite passive microwave sensor AMSR-E. *Remote Sens. Environ.* **112**, 4285–4300 (2008).
19. Tian, F., Brandt, M., Liu, Y. Y., Rasmussen, K. & Fensholt, R. Mapping gains and losses in woody vegetation across global tropical drylands. *Glob. Change Biol.* **23**, 1748–1760 (2017).
20. Wigneron, J.-P. et al. Global carbon balance of the forest: satellite-based L-VOD results over the last decade and perspectives. *Front. Remote Sensing* **5** (2024).
21. Brandt, M. et al. Satellite passive microwaves reveal recent climate-induced carbon losses in African drylands. *Nat. Ecol. Evol.* **2**, 827–835 (2018).
22. Jones, M. O., Jones, L. A., Kimball, J. S. & McDonald, K. C. Satellite passive microwave remote sensing for monitoring global land surface phenology. *Remote Sens. Environ.* **115**, 1102–1114 (2011).
23. Frappart, F. et al. Global monitoring of the vegetation dynamics from the vegetation optical depth (VOD): a review. *Remote Sens.* **12**, 2915 (2020).
24. Li, X. et al. Global-scale assessment and inter-comparison of recently developed/reprocessed microwave satellite vegetation optical depth products. *Remote Sens. Environ.* **253**, 112208 (2021).
25. Loewenstein, N. J. & Pallardy, S. G. Drought tolerance, xylem sap abscisic acid and stomatal conductance during soil drying: a comparison of young plants of four temperate deciduous angiosperms. *Tree Physiol.* **18**, 421–430 (1998).
26. Eziz, A. et al. Drought effect on plant biomass allocation: a meta-analysis. *Ecol. Evol.* **7**, 11002–11010 (2017).
27. Jones, M. O., Kimball, J. S. & Jones, L. A. Satellite microwave detection of boreal forest recovery from the extreme 2004 wildfires in Alaska and Canada. *Glob. Change Biol.* **19**, 3111–3122 (2013).
28. Brando, P. M. et al. Drought effects on litterfall, wood production and belowground carbon cycling in an Amazon forest: results of a throughfall reduction experiment. *Philos. Trans. R. Soc. B* **363**, 1839–1848 (2008).
29. Binks, O. et al. Vapour pressure deficit modulates hydraulic function and structure of tropical rainforests under nonlimiting soil water supply. *N. Phytologist* **240**, 1405–1420 (2023).
30. Giardina, F. et al. Tall Amazonian forests are less sensitive to precipitation variability. *Nat. Geosci.* **11**, 405–409 (2018).
31. Bruno, R. D., Da Rocha, H. R., De Freitas, H. C., Goulden, M. L. & Miller, S. D. Soil moisture dynamics in an eastern Amazonian tropical forest. *Hydrological Process.* **20**, 2477–2489 (2006).
32. Walther, G.-R. et al. Ecological responses to recent climate change. *Nature* **416**, 389–395 (2002).
33. Bennett, A. C. et al. Resistance of African tropical forests to an extreme climate anomaly. *Proc. Natl Acad. Sci. USA* **118**, e2003169118 (2021).
34. Dou, Y. et al. Reliability of using vegetation optical depth for estimating decadal and interannual carbon dynamics. *Remote Sens. Environ.* **285**, 113390 (2023).
35. Wang, X. et al. Globally consistent patterns of asynchrony in vegetation phenology derived from optical, microwave, and fluorescence satellite data. *JGR Biogeosci.* **125**, e2020JG005732 (2020).
36. Du, J. et al. A global satellite environmental data record derived from AMSR-E and AMSR2 microwave Earth observations. *Earth Syst. Sci. Data* **9**, 791–808 (2017).
37. Huete, A. et al. Overview of the radiometric and biophysical performance of the MODIS vegetation indices. *Remote Sens. Environ.* **83**, 195–213 (2002).
38. McDowell, N. et al. Mechanisms of plant survival and mortality during drought: why do some plants survive while others succumb to drought? *N. Phytologist* **178**, 719–739 (2008).
39. Wang, H. et al. Seasonal variations in vegetation water content retrieved from microwave remote sensing over Amazon intact forests. *Remote Sens. Environ.* **285**, 113409 (2023).
40. Hansen, M. C. et al. High-resolution global maps of 21st-century forest cover change. *Science* **342**, 850–853 (2013).
41. Li, X. et al. The first global soil moisture and vegetation optical depth product retrieved from fused SMOS and SMAP L-band observations. *Remote Sens. Environ.* **282**, 113272 (2022).
42. Vicente-Serrano, S. M. et al. Response of vegetation to drought time-scales across global land biomes. *Proc. Natl Acad. Sci. USA* **110**, 52–57 (2013).
43. Gebrechorkos, S. H. et al. Global high-resolution drought indices for 1981–2022. *Earth Syst. Sci. Data* **15**, 5449–5466 (2023).
44. Vicente-Serrano, S. M., Beguería, S. & López-Moreno, J. I. A multiscalar drought index sensitive to global warming: the Standardized Precipitation Evapotranspiration Index. *J. Clim.* **23**, 1696–1718 (2010).
45. Yuan, W. et al. Increased atmospheric vapor pressure deficit reduces global vegetation growth. *Sci. Adv.* **5**, eaax1396 (2019).
46. Beck, H. E. et al. MSWEP V2 Global 3-Hourly 0.1° precipitation: methodology and quantitative assessment. *Bull. Am. Meteorol. Soc.* **100**, 473–500 (2019).
47. Liang, J. et al. Positive biodiversity-productivity relationship predominant in global forests. *Science* **354**, aaf8957 (2016).
48. Lang, N., Jetz, W., Schindler, K. & Wegner, J. D. A high-resolution canopy height model of the Earth. *Nat. Ecol. Evol.* **7**, 1778–1789 (2023).
49. Guglielmetti, M. et al. Measured microwave radiative transfer properties of a deciduous forest canopy. *Remote Sens. Environ.* **109**, 523–532 (2007).
50. Guglielmetti, M., Schwank, M., Mätzler, C., Vanderborght, J. & Flüher, H. FOSMEX: forest soil moisture experiments with microwave radiometry. *IEEE Trans. Geosci. Remote Sensing* **46** (2008).
51. Tian, F. et al. Calibrating vegetation phenology from Sentinel-2 using eddy covariance, PhenoCam, and PEP725 networks across Europe. *Remote Sens. Environ.* **260**, 112456 (2021).
52. Xiang, D. Fitting generalized additive models with the GAM procedure. In *SUGI Proceedings*, 256–326 (Cary NC: SAS Institute, Inc., 2001).
53. Schwalm, C. R. et al. Global patterns of drought recovery. *Nature* **548**, 202–205 (2017).
54. Yao, Y., Liu, Y., Zhou, S., Song, J. & Fu, B. Soil moisture determines the recovery time of ecosystems from drought. *Glob. Change Biol.* **29**, 3562–3574 (2023).
55. Breiman, L. Random Forests. *Mach. Learn.* **45**, 5–32 (2001).
56. Delgado-Baquerizo, M. et al. Climate legacies drive global soil carbon stocks in terrestrial ecosystems. *Sci. Adv.* **3**, e1602008 (2017).
57. Liu, Z., Zhu, J., Xia, J. & Huang, K. Declining resistance of vegetation productivity to droughts across global biomes. *Agric. For. Meteorol.* **340**, 109602 (2023).

Acknowledgements

This work is supported by the National Key Research and Development Program of China (Grant No. 2023YFF1303702), the National Natural Science Foundation of China (Grant No. 42001299), and the Fundamental Research Funds for the Central Universities (1504/600460110).

Author contributions

Yujie Dou contributed to the study design, data collection, data analysis, and drafting of the manuscript. Feng Tian contributed to the study design, the editing of the manuscript, and supervising the project. Jean-Pierre Wigneron and Xiaojun Li contributed to the data collection and editing of the manuscript. Wenmin Zhang, Yaoliang Chen, Luwei Feng, Qi Xie, and Rasmus Fensholt contributed to the editing of the manuscript.

Competing interests

The authors declare no competing interests.

Additional information

Supplementary information The online version contains supplementary material available at <https://doi.org/10.1038/s43247-024-01892-9>.

Correspondence and requests for materials should be addressed to Feng Tian.

Peer review information *Communications Earth & Environment* thanks the anonymous reviewers for their contribution to the peer review of this work. Primary Handling Editors: Alice Drinkwater and Mengjie Wang. A peer review file is available.

Reprints and permissions information is available at <http://www.nature.com/reprints>

Publisher's note Springer Nature remains neutral with regard to jurisdictional claims in published maps and institutional affiliations.

Open Access This article is licensed under a Creative Commons Attribution-NonCommercial-NoDerivatives 4.0 International License, which permits any non-commercial use, sharing, distribution and reproduction in any medium or format, as long as you give appropriate credit to the original author(s) and the source, provide a link to the Creative Commons licence, and indicate if you modified the licensed material. You do not have permission under this licence to share adapted material derived from this article or parts of it. The images or other third party material in this article are included in the article's Creative Commons licence, unless indicated otherwise in a credit line to the material. If material is not included in the article's Creative Commons licence and your intended use is not permitted by statutory regulation or exceeds the permitted use, you will need to obtain permission directly from the copyright holder. To view a copy of this licence, visit <http://creativecommons.org/licenses/by-nc-nd/4.0/>.

© The Author(s) 2024